Malaysian Journal of Catalysis
http://mjcat.utm.my/
MJCat
Research Article

# Effect of Ceria Doped on Fibrous Silica Titania Catalyst for Enhanced Photodegradation of Ciprofloxacin in visible light

Maryam Ibrahim[1*], Aishah Abdul Jalil[2,3], Nursyazwina Norazman[2], Anees Ameera Fauzi[2], Nur Izzati Hannani Binti Hazril[2]

[1]*Department of Chemical Engineering, Abubakar Tafawa Balewa University Bauchi, Nigeria*
[2]*Faculty of Chemical and Energy Engineering, Universiti Teknologi Malaysia, 81310 UTM Johor Bahru, Johor, Malaysia*
[3]*Centre of Hydrogen Energy, Institute of Future Energy, 81310, UTM Johor Bahru, Johor, Malaysia*

**Corresponding Author: maryamibrahim2704@gmail.com*

***Article history:***
*Received 2 January 2026*
*Accepted 30 January 2026*

**ABSTRACT**

Advanced oxidation processes (AOPs) is one of the most promising methods to degrade such organic pollutants from water. Titania ($TiO_2$) is the most attractive semiconductor photocatalyst due to non-toxicity compound and low cost. Notwithstanding, its application is limited owing to the wide band gap, high recombination rate of the charge carriers, low surface area and low absorption of light. This study was focused on the synthesis of different ceria (Ce) loading on fibrous silica titania (FST) by using hydrothermal and impregnation method. The physical and chemical properties of FST-Ce was characterized by X-ray diffraction (XRD), ultraviolet visible spectrophotometer diffuse reflectance spectroscopy (UV-Vis/DRS), field emission scanning electron microscope (FESEM) and fourier transform infrared (FTIR); and the performance of photocatalytic activity was evaluated on the photodegradation of ciprofloxacin (CIP) under different type of catalysts, pH, catalyst dosage and CIP initial concentration. The result revealed that FST-3Ce showed the best performance which is 90% of CIP photodegradation due to low band gap, high crystallinity and strongest interaction between Si-O-Si, Si-OH, and Si-O-M bonds. A kinetic study using Langmuir-Hinshelwood model illustrated that the photodegradation followed the pseudo-first-order and adsorption was the rate-limiting step.

*Keywords*: *Fibrous silica titania, ceria metal loaded, photodegradation, ciprofloxacin, pharmaceutical*


| eISSN 0128-2581 |

## 1. INTRODUCTION

Ciprofloxacin (CIP) belongs to the second-generation fluoroquinolone (FQ's) class of antibiotics and it is used to treat bacterial infections. According to Liu et al (2017), less than 75% of administered CIP is excreted from patient's body in un-metabolized form and ends up into municipal wastewater [1]. Furthermore, CIP gives negative impacts on living things include antibiotic resistance in microorganisms, such as Enterococci sp. and Escherichia coli sp. which can mutate and even become resistant, hence, increase human health risks [2]. To overcome these problems, different treatment processes are approached including advanced oxidation process like ozonation, photolysis and photo-catalysis; coagulation, chemical precipitation and chlorination.

Recently, advanced oxidation processes (AOPs), in particular with heterogenous photocatalysis, have shown tremendous promise as alternatives for wastewater treatment of emerging contaminants [3]. Among photocatalyst, Titania ($TiO_2$) has been widely used in the photodegradation process to generate charge carriers through inducing reductive and oxidative processes respectively [4]. Nevertheless, the practical use of $TiO_2$ is limited by its relatively low surface area, scarcity of accessible active sites, and weak visible-light harvesting capability, highlighting the need for alternative strategies to overcome these limitations [5].

To surmount these problems, several strategies have been developed to increase the photodegradation activity including the deposition of $TiO_2$ on the surface of mesoporous silica which is a simple method for producing active photocatalyst with anatase nanocrystallites dispersed on the huge surface of a $SiO_2$ thermally stable framework. Furthermore, the phase transition anatase to rutile can be delay in the presence of $SiO_2$, which is preferable for photocatalytic properties since rutile is less active than anatase [6]. In addition, some researchers reported that $TiO_2$ doped with rare earth (RE) elements such as cerium, yttrium, lanthanum and neodymium can increase the activity of photocatalytic degradation process compared with undoped $TiO_2$. Although diverse RE ions doped $TiO_2$ photocatalysts

have been successfully prepared, there is a shortage of erudition regarding the influence of the radii of RE ions on the photocatalytic properties. Furthermore, RE-doped $TiO_2$ has low photocatalytic efficiency and it also difficulty in being recovered [7].

In this work, the synthesis and characterization of fibrous silica titania (FST) doped with different weight of ceria (Ce) was conducted. The charazterization of the catalysts were studied by XRD, UV-Vis/DRS, FTIR AND FESEM. The performance of synthesized catalysts towards the photodegradation of ciprofloxacin (CIP) was evaluated and the potential of the catalyst was investigating under different parameters such as pH (3-9), catalyst dosage (0-0.5 g $L^{-1}$) and initial concentrations (10-100 mg $L^{-1}$). The kinetics and stability of the catalysts are also discussed.

## 2. EXPERIMENTS

### 2.1 Materials

The Cetyltrimethylammonium bromide, CTAB $\{(C_{16}H_{33})N(CH_3)_3BR^-\}$ with greater than 99% purity was used as surfactant and were obtained from MERCK, Urea $(CO(NH_2)_2)$ with greater than 99.5% as hydrolyzing agent and Toluene ($C_7H_8$) as oil phase were purchased from QREC™ . 1-Butanol ($C_4H_9OH$) with greater than 99.5% purity which used as co-surfactant and Cerium (III) nitrate hexahydrate ($Ce(NO_3)_3$ were obtained from Sigma Aldrich. Tetraethyl orthosilicate. TEOS $\{Si(OC_2H_5)_4\}$ with greater than 98% purity was used as precursor which purchased from Acros Organics and Titania (JRC $TiO_2$) was used as Titania sources. Ciprofloxacin ($C_{17}H_{18}FN_30_3$) with greater than 98% purity as pollutant was purchased from TCI.

### 2.2 Preparation of catalyst

Fibrous silica titania (FST) was synthesized by using hydrothermal method. 24.65 g of CTAB and 14.73 g of urea was mixed in 732 mL of distilled water, stirred for 5 min at 800-900 rpm. Next, 623.6 mL of toluene and 36.8 mL of 1-butanol were added into the mixture and stirred for another 15 min at room temperature. After that, 5.9 g of titania seed was added into the mixture and stirred for another 30 min. Subsequently, 55.6 mL of TEOS was added drop wise and the mixture was stirred for 2 hours at room temperature. After 2 hours stirring, the resulting mixture was heated in oven for 6 hours at 120℃. After heating the product was dried overnight at 110℃ before calcination at 550℃ for 6 hours.

Then, different loading Ce catalysts (1wt %, 3wt %, 5wt % and 7wt %) were prepared by incipient wetness impregnation method. General preparation steps for monometallic loaded FST catalysts as follows. The specific amount of Cerium (III) nitrate hexahydrate was dissolved into the distilled water and mixed with the catalyst support (FST). The mixture was heated at 353 K under continuous stirring until the formation of the thick paste. The as-synthesized catalyst was dried at 383K overnight and calcined at 823 K for 3 hours.

### 2.3 Photocatalytic degradation of RhB

The photoactivity of the catalysts were examined on the degradation of CIP. A batch reactor fixed with cooling system and 4 units of UV lamp (9 W; 254 nm) was used in this experiment. A catalyst (0.375 g $L^{-1}$) was put in the beaker containing 100 mL CIP solution. Then, the solution was stirred in the dark for 30 min to achieve equilibrium of the adsorption-desorption before being radiated with light for 4 h. The initial concentration and pH of CIP solution were 10 mg $L^{-1}$ and pH3, respectively. At regular interval of 30 min, the sample were collected and centrifuged. The CIP adsorption band was analyzed at 246 nm using UV-Vis spectrophotometry (Agilent Technologies, Cary 60 UV-Vis, USA) and the following equation was used to determine CIP degradation percentage.

$$Degradation(\%) = \frac{Co - C_t}{Co} \times 100$$

where $C_o$ is the initial concentration of CIP and $C_t$ is the concentration at time t.

### 2.4 Characterization

The microscopic surface morphology of the prepared photocatalysts was evaluated through a field-emission scanning electron microscope (FESEM). The optical absorbance was recorded via ultraviolet-visible/diffuse reflectance spectra (UV-Vis/DRS) spectrophotometer and the extrapolation of bandgap photocatalysts. The crystallinity of the catalysts was determine using X-ray Diffraction (XRD). The chemical functional group of the photocatalyst was measured using Fourier transform infrared (FTIR) via the KBr method.

### 2.5 Stability test

The experiment was repeated to study the reusability of the catalyst. 0.500 g of the synthesized catalyst was dispersed into 1000 mL of 10 mg $L^{-1}$ CIP with pH 3 using a batch reactor fixed with a cooling system. The solution was stirred in the dark for 30 min and then exposed under visible light for another 4 hours. During the process, 1.5 mL of CIP solution samples was collected every 15 min using a tube connected with syringe and centrifuged using Beckman Coulter Microfuge 16 Centrifuge at 14,000 rpm for 10 min. Subsequently, the concentration of centrifuged CIP was analyzed by UV-Vis spectrophotometer (Cary 60 UV-Vis Agilent) at absorption band between (276-278) nm. For a new cycle, the mixture of CIP solution and photocatalyst was centrifuged and the collected catalyst was washed, dried in the oven overnight at 110℃ and calcined at 550℃ for 6 hours before being regenerated for degrading of the next fresh CIP solution. All of the reaction parameters

were kept constant with five regeneration cycles for stability study.

## 3. RESULTS AND DISCUSSION

### 3.1 Characterization of photocatalysts

#### 3.1.1 Crystallinity and Phase Study

Figure 1A and B shows a wide angle XRD diffractogram of the commercial $CeO_2$, and synthesized of FST-Ce with different ceria (Ce) wt% loading, respectively. Based on Figure 1A, a series of characteristic peak were observed at 28.6˚ (1 1 1), 33.1˚ (2 0 0), 47.6˚ (2 2 0), 56.3˚ (3 1 1) and 69.4˚ (4 0 0) which indicates the pure cubic fluorite structure (JCPDS No: 34-0394[8, 9]. Besides that, Figure 1B illustrated the FST catalyst and the peak intensity were identified at 25.4˚ (1 0 1), 37.8˚ (0 0 4), 38.6˚ (1 1 2), 48˚ (2 0 0), 53.9˚ (1 0 5) and 55.1˚ (2 1 1) which can assign as anatase phase because of typical peak of $TiO_2$ (JCPDS file No. 01-086-1157) [10].

Regarding to Figure 1B, after Ce was loaded on FST catalyst, a new diffraction peak was discovered at 28.6˚ (1 1 1) which indicated Ce was a successful loading and the FST peak was still maintained at 25.4˚ (1 0 1), 37.8˚ (0 0 4), 38.6˚ (1 1 2), 48˚ (2 0 0), 53.9˚ (1 0 5) and 55.1˚ (2 1 1). As the Ce loading increase, it was observed that the peak at 28.6˚ (1 1 1) become lower. However, the diffraction peak for FST is maintained consistent last on FST-3Ce, as the peak intensity of FST at 25.4˚ (1 0 1) for FST-7Ce was started to decrease after increasing the Ce loading. Hence, FST-3Ce shows the highest crystallinity of FST catalyst while containing Ce.

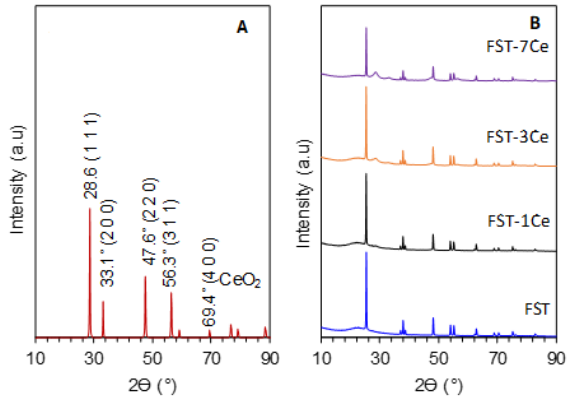


Figure 1. XRD patterns of commercial of A) CeO2 B) FST, FST-1Ce, FST-3Ce and FST-7Ce catalysts.

#### 3.1.2 Band Gap Determination

Band gap of the photocatalyst plays an important key role in order to utilize photocatalytic applications. The catalysts were then subjected to UV-Vis DRS to analyse band gap energy. The band-gap of the samples was calculated using the equation of $E = 1240/\lambda$, where E is the band gap energy in eV and λ is the wavelength in nanometer [11]. The summary of the band gap for all catalysts is stated in Table 1. FST-3Ce showed lower band gap energy (2.94 eV) compared to FST (3.18 eV). The reduction of band gap after Ce doped on FST is might be due to the more formation of surface defect [12]. While, among all Ceria loaded catalysts, FST-3Ce showed lower band gap energy and this result led to the potential use of it in visible light responsive photocatalytic reaction.

**Table 1 Band gap of the catalysts**

| Catalyst | Band gap (eV)[a] |
|---|---|
| FS-3Ce | 3.06 |
| FST | 3.18 |
| FST-1Ce | 2.90 |
| FST-3Ce | 2.94 |
| FST-5Ce | 3.02 |
| FST-7Ce | 3.10 |

[a]Calculated from Kulbelka-Munk

#### 3.1.3 Morphological Study

The morphologies of FST and FST-3Ce under field emission scanning electron microscopy (FESEM) are shown in Figure 2A and B, respectively. It was observed that a well cockscomb-like structured of both catalysts were successfully synthesized by hydrothermal method. Based on the FESEM images, the average sizes of FST and FST-3Ce were found to be 636.36 and 527.27 nm, respectively. The size of FST-3Ce catalyst is smaller compared to FST catalyst. This might be due to either Ce loading caused lattice deformation and generation of oxygen vacancies, or to the formation of disparate boundaries which restrains the crystal growth [13].

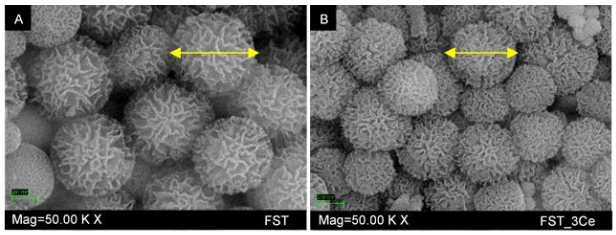


Figure 2. FESEM images of A) FST and B) FST-3Ce at magnification 50.00 K X

#### 3.1.4 Fourier Transform Infrared (FTIR) Spectroscopy

For chemical properties studies, all the samples catalysts were then characterized by FTIR and the spectra in the region of 4000 - 400 $cm^{-1}$ are shown in Figure 3A. Several major absorption bands were seen at 3400, 1084,

966, 790 and 460 $cm^{-1}$ which attributed to the presence of -OH stretching, Si-O-Si asymmetric, external Si-OH group, Si-O-Si asymmetric stretching and Si-O-Si bending vibration [14]. Figure 3B and C illustrates the summarized band intensity obtained from FTIR spectra. Figure 3B clearly shows that the intensity bands of FST-3Ce is the highest compared to others particularly at 3400 and 1084 $cm^{-1}$. The increase of ceria loading up to 3 wt% is resulted in increased intensity of these both peaks. This indicates that the introduction of ceria makes the catalyst possess more surface hydroxyl groups. The hydroxyl groups play an important role in the photocatalytic reaction since they can capture the photoinduced holes and then form hydroxyl radicals with high oxidation capability [15]. Besides that, the increase of peak at 1084 $cm^{-1}$ is due to strong interaction occurred between the added metal and $SiO_2$ framework of FS and possible formation of new Si-O-Si bonds.

The band in the range of 900-1000 $cm^{-1}$ illustrated the significant region usually involved in the rearrangement of the $SiO_2$ network subsequent to alteration [16, 17, 18]. As shown in Figure 3C, the band at 935, 948 and 965 $cm^{-1}$ was assigned to Si-O-Ti bond, non-bridging free broken Si-O stretching and Si-O-H stretching, respectively. Among all catalysts, FST-3Ce shows the strongest interaction between Si-O-Si, Si-OH and Si-O-M bonds.

## 3.2 Photocatalytic degradation of CIP

### 3.2.1 Performance of the Synthesized Photocatalysts

The photocatalytic performance of the synthesized catalysts was evaluated on the degradation of ciprofloxacin (CIP) with the result shown in Figure 4A and B under visible light irradiation for 240 minutes. FST-3Ce (90%) catalyst was exhibited the highest photocatalytic performance among the prepared catalyst (FS-3Ce (59%), FST (79%), FST-1Ce (78%), FST-5Ce (73%) and FST-7Ce (70%)) due to narrowing of its band gap which can lead to decrease in electron-hole recombination rate [19]. Notably, FST-3Ce showed ~5.3-fold higher activity than pristine $CeO_2$ (90% vs 17%), confirming the beneficial role of Ce incorporation within the FST framework.

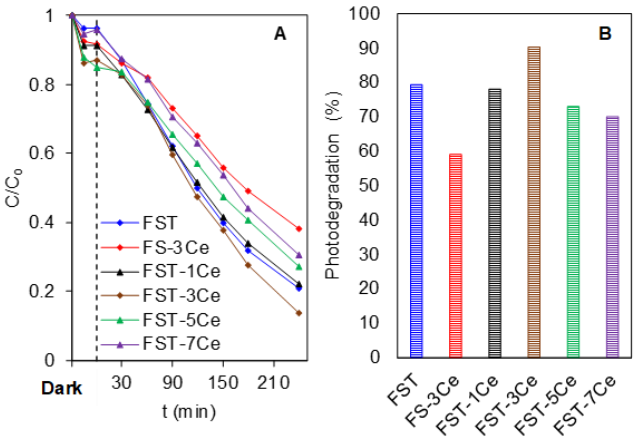


Figure 4. Photodegradation of CIP of A) $C/C_o$ versus t graph and B) percentage graph using different type of catalyst (Reaction condition: Visible light, t=240 min, W=0.375 g $L^{-1}$, $[CIP]_0$ =10 $mgL^{-1}$, pH 3)

### 3.2.2 Effects of pH

In the photocatalytic activity, pH plays a crucial role for the removal efficiency of CIP. In advanced oxidation processes, pH can have a large influence on the removal rate of the contaminant, absorption capacity, distribution of electric charge on the catalyst surface, and oxidation potential of the valence band [20]. Herein, the effect of pH on photodegradation of CIP was investigated ranging from of 3-9 in the presence of the FST-3Ce catalyst and the results

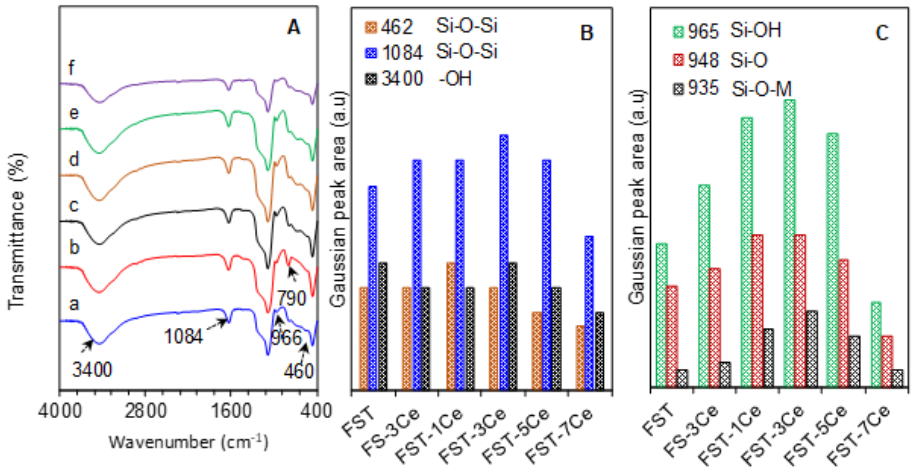


Figure 3. A) FTIR spectra of (a)FST (b) FS-3Ce (c) FST-1Ce (d) FST-3Ce (e) FST-5Ce and (f) FST-7Ce, B) Peak intensity of FTIR spectra at 462 $cm^{-1}$, 1084 $cm^{-1}$ and 3400 $cm^{-1}$ C) Peak intensity of FTIR spectra at 965 $cm^{-1}$, 948 $cm^{-1}$ and 935 $cm^{-1}$.

are shown in Figure 5. Figure 5B shows that the photocatalytic reaction by using FST-3Ce catalyst after 240 minutes under visible light irradiation was achieved 90%, 58%, 47% and 32% at pH 3, 5, 7 and 9 respectively. Based on the result, it was found that the increase in pH values causes reducing the photodegradation performance of CIP.

Moreover, in fact, this behaviour can be described on the basis of the point zero charge ($pH_{pzc}$) of the FST-3Ce, which was determined to be at pH 3 as shown in Figure 5A. It is well-known that for pH values higher than $pH_{pzc}$, the surface becomes negatively charged and vice versa for pH < $pH_{pzc}$. Therefore, the positively charged CIP would be strongly attracted to the negatively charged FST-3Ce catalyst surface at pH > $pH_{pzc}$ leading to strong absorption and reduction with a corresponding high rate of CIP degradation [21].

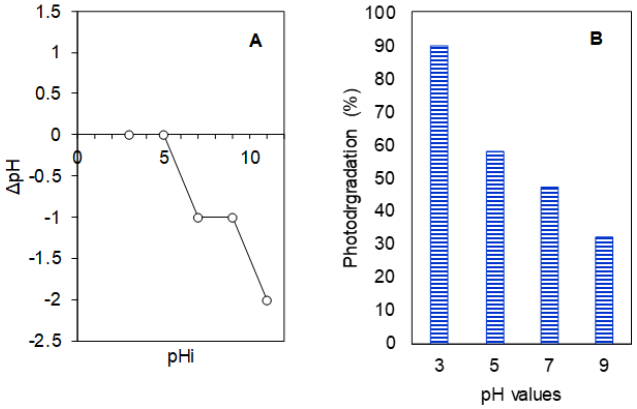


Figure 5. A) $pH_{pcz}$ of FST-3Ce and B) Photodegradation of CIP using FST-3Ce with various pH values of water pollutant (Reaction condition: Visible light, t=240 min, $[CIP]_0$ =10 $mgL^{-1}$, W= 0.375 g $L^{-1}$).

3.2.2 Effects of catalyst dosage

Figure 6 shows the effect of FST-3Ce dosage for photodegradation of CIP. It can be observed that the photocatalytic activity increasing until reaching the optimum dosage which is 0.5$gL^{-1}$, where the photocatalytic performance is 93% and then at 0.75$gL^{-1}$ the CIP degradation performance decrease to 67% due to after the optimum catalyst loading is accomplished. This is because any further increase in the amount of catalyst dose results in photocatalyst aggregation in the solution which will lead to the turbidity of the solution. Nevertheless, the number of active sites and the formation of reactive oxygen species (ROS) will increase correspondingly when the amount of catalyst dosage increased [2].

3.2.2 Effects of CIP initial concentration

The initial concentration of CIP is one of the driving parameters in photodegradation of CIP. The effect of the initial concentration on CIP degradation was studied by preparing different amount of CIP solutions (10-70 $mgL^{-1}$). Based on Figure 7A, the photocatalytic activity will decrease with the increase in the initial concentration of CIP over constant catalyst loading due to it can be attributed to the insufficient number of vacancies for the higher amount of incoming CIP molecules [2]. Furthermore, the penetration of light to reach the surface of the catalyst was hindered which was most likely due to the accumulation of pollutant covering the catalyst surface [17, 22]. Similar report was recorded by Khodadadi *et al.*, (2018) on the influence of tetracycline initial concentration on the photodegradation of tetracycline by $FeNi_3@SiO_2@TiO_2$ nanocomposite [3].

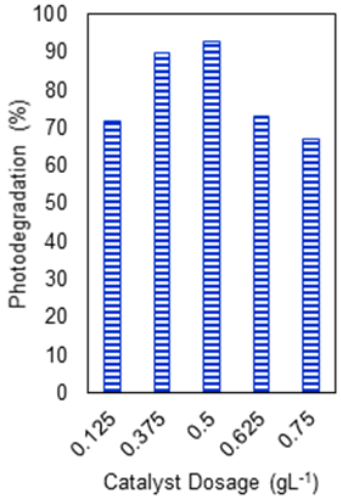


Figure 6. Photodegradation of CIP using FST-3Ce with different catalyst dosage (Reaction condition: Visible light, t=240 min, $[CIP]_0$ =10 $mgL^{-1}$, pH 3).

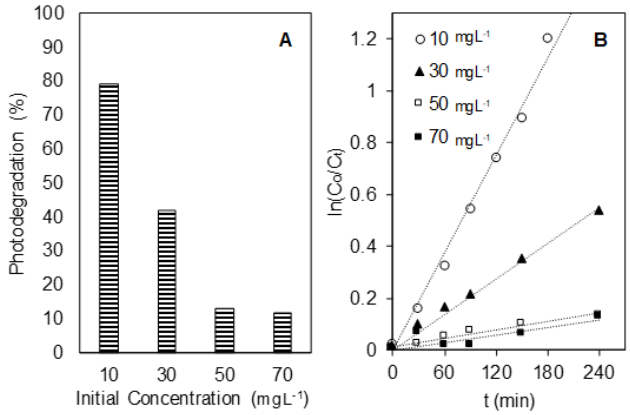


Figure 7. Photodegradation of CIP using FST-3Ce A) with different initial concentrations of CIP and B) photodegradation kinetics of CIP using FST-3Ce at different initial concentrations (Reaction condition: Visible light, t=240 min, W=0.5 g $L^{-1}$, pH 3).

In general, the kinetics of most organic compounds that undergo photocatalytic reactions are described by a pseudo first-order model, which is rationalised in terms of the Langmuir-Hinshelwood model modified to accommodate reactions occurred at the solid-liquid interface [23, 24]. At low initial CIP concentration, the simplest

equation for the rates of photodegradation of CIP is given by the equation below,

$$\ln C_t = -kt + \ln C_o \quad (2)$$

where k is the pseudo first-order rate while $C_o$ and $C_t$ are the concentrations of CIP initially and at time t, respectively. The integration of (Equation 2) yields the (Equation 3),

$$\ln\left(\frac{C_o}{C_t}\right) = kt \quad (3)$$

The linearity of the plot of ln ($C_o$ / $C_t$) vs. irradiation time shown in Figure 7B verified that the reaction process followed the pseudo-first order kinetics model. The slope of the line was the apparent first-order rate constant ($k_{app}$), and the value obtained (Table 2) demonstrated a significant and favourable effect of the FST-3Ce on the photodegradation of CIP. The values of $k_{app}$ decreased with increasing initial concentration, indicating that the system is favorable at low concentration [18]. At lower concentration, the reaction rate is able to control the mechanism since the active sites on the catalyst's surface were only partially occupied by adsorbed CIP molecules. However, the increasing of initial concentration has led to the saturation of the active sites preventing the adsorption of new CIP molecules before the desorption of the degradation by-products [25]. Thus, at higher concentrations, hydroxyl radicals become the limiting reactant, and consequently, lowering the reaction rate. The line with an intercept of $1/k_r$ and $1/kr\ K_{LH}$ was obtained from the Langmuir Hinshelwood (L-H) kinetic formula (Equation 4),

$$\frac{1}{k_{app}} = \frac{1}{k_r K_{LH}} + \frac{C_o}{k_r} \quad (4)$$

where $k_r$ is the reaction rate constant (mg $L^{-1}$ $min^{-1}$), $K_{LH}$ is the adsorption coefficient of the reactant (L $mg^{-1}$) and $C_o$ is the initial concentration of CIP (mg $L^{-1}$). The calculated values of $k_r$ and $K_{LH}$ were 0.102 mg $L^{-1}$ and 0.0511 mg $L^{-1}$, respectively. These results illustrated that since $k_r$, >$K_{LH}$, it was suggested that the CIP adsorption on the surface of FST-Ce was manipulated by the photodegradation process [26].

3.2.5 Proposed Photodegradation Mechanism

Based on the performance and characterization, the structures of the FST-Ce catalyst were proposed as shown in Figure 7. When light is irradiated to the catalyst surface, the electrons at valence band (VB) for both site which is FST and Ceria were excited to its conduction band (CB), leaving behind holes ($H^+$) in VB [27]. The overall reaction occurred during the water splitting reaction as there is reduction of photons using excited electrons present at the CB which will generate Hydrogen gas ($H_2$) and water oxidation using the holes at VB where the oxygen evolution reaction at VB generates some reaction intermediates and protons which also contribute to $H_2$ generation [19].

Ceria can be as electron acceptor due to it has +1, +3 and +4 oxidation states that make cerium cations to be an attractive species [27]. Hence, the photogenerated electrons at CB of FST will be transferred to CB of Ceria. The electron was then reacting with molecular oxygen ($O_2$) to produce superoxide radical anions (• $O_2^-$) and the holes react with water to produce hydroxyl radicals (•OH). These two reactive radicals cooperate together in decomposing CIP to form harmless product.

3.2.5 Stability Test

The potential of catalyst to be recovered and reused in photocatalytic reaction is a great concern since it can contribute to lower operational cost of processes, thus making the photocatalysis as an attractive method for wastewater treatment [28-29]. Hence, a repeated experiment was carried out using FST-3Ce catalyst to study the stability of the catalyst towards CIP degradation as shown in Figure 8. It was found that the FST-3Ce catalyst was still active even after five runs, with only a slight decrease in percentage of degradation. The decrease in photocatalytic efficiency might be due to the heat treatment that caused the catalyst aggregation, thus decreasing the surface area of catalyst [30]. Thus, it was suggested that the FST-3Ce is a stable photocatalyst and is not easily deactivated during the degradation process.

Table 2 The kinetics parameters of photodegradation process

| **Initial concentration of CIP, Co (mg $L^{-1}$)** | **Degradation (%)** | **Reaction rate, kapp (x $10^{-2}$mg $L^{-1}$$min^{-1}$)** | **Initial rate, $r_o$ (x $10^{-1}$mg $L^{-1}$$min^{-1}$)** |
|---|---|---|---|
| 10 | 92.57 | 0.43 | 0.43 |
| 30 | 41.74 | 0.18 | 0.54 |
| 50 | 12.71 | 0.14 | 0.70 |
| 70 | 11.89 | 0.12 | 0.84 |

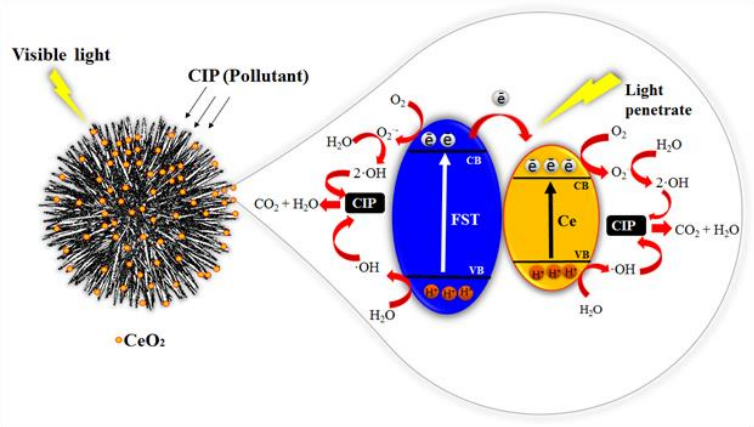


Figure 8 Illustration of proposed mechanism for CIP photodegradation

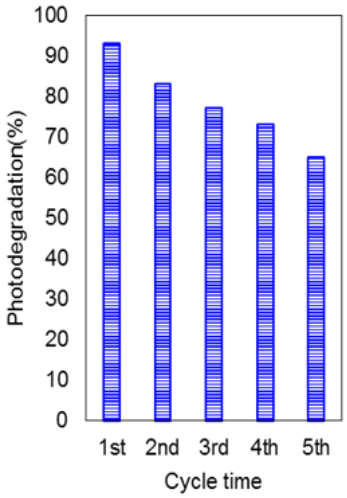


Figure 9. Stability of FST-3Ce on photodegradation of CIP (Reaction condition: Visible light, t= 240 min, $[CIP]_0$=10 $mgL^{-1}$, W = 0.5 $gL^{-1}$, pH 3)

## 4. CONCLUSION

In this investigation, ceria loaded on FST (FST-Ce) was successfully synthesized by a hydrothermal and impregnation method under various weight percent of ceria, which were then characterized. Regarding on the characterization results, the ceria loaded on FST caused decreasing the particle size due the formation of distinct boundaries which limits the crystal growth. Among all the catalysts, FST-3Ce showed the strongest interaction between Si-O-Si, Si-OH, and Si-O-M bonds. The photocatalytic performance of the catalysts towards degradation of 10 mg $L^{-1}$ of CIP at pH 3 and 0.5 g $L^{-1}$ catalyst for 4 hours under visible light was in the following order: FST-3Ce (90%)> FST (79%)> FST-1Ce (78%)> FST-5Ce (73%)> FST-7Ce (70%) > FSCe (73%). FST-3Ce shows the highest photocatalytic performance due to narrow band gap, high crystallinity and interaction as mentioned above. The kinetics study revealed that the photodegradation process is determined by the Langmuir-Hinshelwood model which has followed the pseudo first-order. The results illustrated that $k_r$ (0.102 mg $L^{-1}$) > $K_{LH}$ (0.0511 mg $L^{-1}$), suggesting that the CIP adsorption on the surface of FST-Ce was manipulated of the photodegradation process. The stability test signified that the catalyst remained stable after five cycles.

## ACKNOWLEDGEMENTS

The authors are grateful for the financial support from Kurita Water and Environment Foundation Research Grant Program 2023 (grant number 4J652).

## REFERENCES

[1] Liu, L., Mi, J., Wang, Y., Zou, Y., Ma, B., Liao, X., … Wu, Y. (2018). Different methods of incorporating ciprofloxacin in soil affect microbiome and degradation of ciprofloxacin residue. Science of the Total Environment.

[2] Rashid, J., Abbas, A., Chang, L. C., Iqbal, A., Haq, I. U., Rehman, A., … Barakat, M. A. (2019). Butterfly cluster like lamellar BiOBr/TiO2 nanocomposite for enhanced sunlight photocatalytic mineralization of aqueous ciprofloxacin. Science of the Total Environment, 665, 668–677.

[3] Khodadadi, M., Ehrampoush, M. H., Ghaneian, M. T., Allahresani, A., & Mahvi, A. H. (2018). Synthesis and characterizations of FeNi 3 @ SiO 2 @ TiO 2 nanocomposite and its application in photo- catalytic degradation of tetracycline in simulated wastewater. 255, 224–232.

[4] Gaya, U. I., & Abdullah, A. H. (2008, March). Heterogeneous photocatalytic degradation of organic contaminants over titanium dioxide: A review of fundamentals, progress and problems. Journal of Photochemistry and Photobiology C: Photochemistry Reviews, Vol. 9, pp. 1–12.

[5] Rivero, M. J., Iglesias, O., Ribao, P., & Ortiz, I. (2019). Kinetic performance of TiO2/Pt/reduced graphene oxide composites in the photocatalytic hydrogen production. International Journal of Hydrogen Energy.

[6] Lebeau, B., Bonne, M., Comparot, J. D., Rousseau, J., Michelin, L., Blin, J. L., & Brunet, S. (2019). HDS of

4,6-dimethyldibenzothiophene over CoMoS supported mesoporous SiO 2 -TiO 2 materials. Catalysis Today.

[7] Zhou, F., Yan, C., Sun, Q., & Komarneni, S. (2019). TiO2/Sepiolite nanocomposites doped with rare earth ions: Preparation, characterization and visible light photocatalytic activity. Microporous and Mesoporous Materials, 274(May 2018), 25–32.

[8] Chelliah, M., Rayappan, J. B. B., & Krishnan, U. M. (2012). Synthesis and characterization of cerium oxide nanoparticles by hydroxide mediated approach. Journal of Applied Sciences.

[9] Zhou, L., Li, X., Yao, Z., Chen, Z., Hong, M., Zhu, R., … Zhao, J. (2016). Transition-Metal Doped Ceria Microspheres with Nanoporous Structures for CO Oxidation. Scientific Reports.

[10] Jaafar, N. F., Jalil, A. A., & Triwahyono, S. (2017). Visible-light photoactivity of plasmonic silver supported on mesoporous TiO2 nanoparticles (Ag-MTN) for enhanced degradation of 2-chlorophenol: Limitation of Ag-Ti interaction. Applied Surface Science.

[11] Rani, N., Ahlawat, R., & Goswami, B. (2020). Annealing effect on bandgap energy and photocatalytic properties of CeO2–SiO2 nanocomposite prepared by sol-gel technique. Materials Chemistry and Physics, 241, 122401.

[12] Bhushan, M., Jha, R., & Bhardwaj, R. (2019). Reduced band gap and diffusion controlled spherical n-type ZnS nanoparticles for absorption of UV-Vis region of solar spectrum. Journal of Physics and Chemistry of Solids, 135, 109021.

[13] Fu, C., Gong, Y., Wu, Y., Liu, J., Zhang, Z., Li, C., & Niu, L. (2016). Photocatalytic enhancement of TiO 2 by B and Zr co-doping and modulation of microstructure. Applied Surface Science.

[14] Mortazavi-Derazkola, S., Salavati-Niasari, M., Amiri, O., & Abbasi, A. (2017). Fabrication and characterization of Fe3O4@SiO2@TiO2@Ho nanostructures as a novel and highly efficient photocatalyst for degradation of organic pollution. Journal of Energy Chemistry, 26(1), 17–23.

[15] Hao, Z. and Iqbal, A. (1997). Some aspects of organic pigments. *Chemical Society Reviews*, 26(3): 203-213

[16] Salleh, N. F. M., Jalil, A. A., Triwahyono, S., Efendi, J., Mukti, R. R., & Hameed, B. H. (2015). New insight into electrochemical-induced synthesis of NiAl2O4/Al2O3: Synergistic effect of surface hydroxyl groups and magnetism for enhanced adsorptivity of Pd(II). Applied Surface Science, 349, 485–495.

[17] Jusoh, R., Jalil, A. A., Triwahyono, S., & Kamarudin, N. H. N. (2015). Synthesis of dual type Fe species supported mesostructured silica nanoparticles: Synergistical effects in photocatalytic activity. RSC Advances.

[18] Hitam, C. N. C., Jalil, A. A., Triwahyono, S., Ahmad, A., Jaafar, N. F., Salamun, N., … Ghazali, Z. (2016). Synergistic interactions of Cu and N on surface altered amorphous TiO2 nanoparticles for enhanced photocatalytic oxidative desulfurization of dibenzothiophene. RSC Advances.

[19] Ameen Sha, M., Chandrasekharan Meenu, P., Sasidharan Sumi, V., Chithrajakumary Bhagya, T., Revamma Sreelekshmy, B., & Shibli, S. M. A. (2020). Tuning of electron transfer by Ni–P decoration on CeO2–TiO2 heterojunction for enhancement in photocatalytic hydrogen generation. Materials Science in Semiconductor Processing.

[20] Nasseh, N., Taghavi, L., Barikbin, B., & Ali, M. (2018). Synthesis and characterizations of a novel FeNi3 / SiO2 / CuS magnetic nanocomposite for photocatalytic degradation of tetracycline in simulated wastewater. Journal of Cleaner Production, 179, 42–54.

[21] Li, F., Kang, Y., Chen, M., Liu, G., Lv, W., Yao, K., … Huang, H. (2016). Photocatalytic degradation and removal mechanism of ibuprofen via monoclinic BiVO4 under simulated solar light. Chemosphere.

[22] Khusnun, N. F., Jalil, A. A., Triwahyono, S., Jusoh, N. W. C., Johari, A., & Kidam, K. (2016). Interaction between copper and carbon nanotubes triggers their mutual role in the enhanced photodegradation of: P - chloroaniline. Physical Chemistry Chemical Physics.

[23] Jaafar, N. F., Jalil, A. A., Triwahyono, S., & Shamsuddin, N. (2015). New insights into self-modification of mesoporous titania nanoparticles for enhanced photoactivity: Effect of microwave power density on formation of oxygen vacancies and Ti3+ defects. RSC Advances.

[24] Jaafar, N. F., Jalil, A. A., Triwahyono, S., Efendi, J., Mukti, R. R., Jusoh, R., … Suendo, V. (2015). Direct in situ activation of Ag0 nanoparticles in synthesis of Ag/TiO2 and its photoactivity. Applied Surface Science, 338, 75–84.

[25] Klauson, D., Babkina, J., Stepanova, K., Krichevskaya, M., & Preis, S. (2010). Aqueous photocatalytic oxidation of amoxicillin. Catalysis Today.

[26] Hassan, N. S., Jalil, A. A., Triwahyono, S., Hitam, C. N. C., Rahman, A. F. A., Khusnun, N. F., … Prasetyoko, D. (2018). Exploiting copper–silica–zirconia cooperative interactions for the stabilization of tetragonal zirconia catalysts and enhancement of the visible-light photodegradation of bisphenol A. Journal of the Taiwan Institute of Chemical Engineers.

[27] Chen, Y., Wang, Z., Zhang, Y., Zhou, J., & Cen, K. (2010). Platinum-ceria-zirconia catalysts for hydrogen production in sulfur-iodine cycle. International Journal of Hydrogen Energy.

[28] Saadon, S., Sathishkumar, P., Mohd Yusoff, A. R., Hakim Wirzal, M. D., Rahmalan, M. T., & Nur, H. (2016). Photocatalytic activity and reusability of ZnO layer synthesised by electrolysis, hydrogen peroxide and heat treatment. Environmental Technology (United Kingdom).

[29] Rahman, A. F. A., Jalil, A. A., Triwahyono, S., Ripin, A., Aziz, F. F. A., Fatah, N. A. A., … Hassan, N. S. (2017). Strategies for introducing titania onto mesostructured silica nanoparticles targeting enhanced

photocatalytic activity of visible-light-responsive Ti-MSN catalysts. Journal of Cleaner Production.

[30] Mustapha, F. H., Jalil, A. A., Mohamed, M., Triwahyono, S., Hassan, N. S., Khusnun, N. F., … Zolkifli, A. S. (2017). New insight into self-modified surfaces with defect-rich rutile TiO 2 as a visible-light-driven photocatalyst. Journal of Cleaner Production.